JOURNAL OF AGRICULTURAL AND FOOD CHEMISTRY

Mango Starch Degradation. I. A Microscopic View of the Granule during Ripening

RENATA ANTOUN SIMÃO,[‡] ANA PAULA FIORAVANTE BERNARDES SILVA,[†] FERNANDA HELENA GONÇALVES PERONI,[†] JOÃO ROBERTO OLIVEIRA DO NASCIMENTO,[†] RICARDO PEREIRA LOURO,[§] FRANCO MARIA LAJOLO,[†] AND BEATRIZ ROSANA CORDENUNSI*,[†]

Laboratório de Química, Bioquímica e Biologia Molecular de Alimentos, Departamento de Alimentos e Nutrição Experimental, FCF, Universidade de São Paulo, Avenida Lineu Prestes 580, Bloco 14, CEP 05508-900, São Paulo - SP, Brazil, Programa de Engenharia Metalúrgica e de Materiais, COPPE, Universidade Federal do Rio de Janeiro, CT - F 209, Cidade Universitária, Ilha do Fundão, Caixa Postal 68.505, 21945-970, Rio de Janeiro - RJ, Brazil, and Instituto de Biologia, Dep. Botânica, Laboratório de Ultraestrutura Vegetal, Universidade Federal do Rio de Janeiro, CCS, Cidade Universitária, Ilha do Fundão, 21941-590, Rio de Janeiro - RJ, Brazil

The starch content of unripe mango Keitt is around 7% (FW), and it is converted to soluble sugars during the ripening of the detached fruit. Despite the importance of starch-to-soluble sugar metabolism for mango quality, little literature is found on this subject and none concerning the physical aspects of starch degradation. This manuscript presents some changes in the physical aspects of the starch granule during ripening, as analyzed by light microscopy, scanning electron microscopy (SEM), and atomic force microscopy (AFM). According to the analysis, unripe Keitt-mango-starch being spherical in shape and measuring around 15 μm, has A-type X-ray diffraction pattern with a degree of crystallinity around 21% with slight changes after 8 days of ripening. AFM images of the surface of the granules showed ultra microstructures, which are in agreement with a blocklet-based organization of the granules. The AFM-contrast image of growing layers covering the granule showed fibril-like structures, having 20 nm in diameter, transversally connecting the layer to the granule. The appearance of the partially degraded granules and the pattern of degradation were similar to those observed as a result of amylase activity, suggesting a hydrolytic pathway for the degradation of starch from mango cultivar Keitt. These results provide clues to a better understanding of starch degradation in fruits.

KEYWORDS: Mango; fruit ripening; starch granule; microscopy; starch degradation

INTRODUCTION

Mango Keitt accumulates around 7% of starch during development, while an expressive amount of sucrose is achieved during ripening, simultaneous to starch degradation. Other soluble sugars found in the fruit are glucose and fructose, but in lower amounts than sucrose. The main change of the starch-to-sugar metabolism occurs only after harvest, which turns Keitt into a peculiar cultivar since starch degradation usually starts before harvesting in other mango cultivars (*1*). Despite the importance of starch-to-soluble sugar metabolism, literature about mango fruits is scarce, which may be due to the fact that the cultivar and its maturity stages are not so clear. Keitt presents a typical climacteric behavior as previously presented by Bernardes-Silva et al. (*2*).

Although starch degradation has been extensively studied in previous years, the nature and regulation of the process are yet to be understood. The most well-known process of starch degradation is the one that takes place during cereal endosperm germination. Another well-studied process occurs in leaves, at the mobilization of transitory starch (*3*). However, advances in the degradation process during ripening are limited by the fact that fruit is still living tissue (as opposed to seed endosperm, which is not) and the fact that accumulated starch is not transitory in the sense of being extensively degraded during the light/dark cycle.

Even though starch consists almost solely of glucose molecules, there is a high diversity in the granule shape, size, and degree of crystallinity (A or B type), and also in the amylose/amylopectin proportion, depending on the botanical source. Different granule size can indicate a variation in the molecular structure of the amylopectin fractions (*4*). Besides differences

* Corresponding author. Tel: +55-11-30913656. Fax: +55-11-38154410. E-mail: hojak@usp.br.
[†] Universidade de São Paulo.
[‡] Programa de Engenharia Metalúrgica e de Materiais, Universidade Federal do Rio de Janeiro.
[§] Instituto de Biologia, Universidade Federal do Rio de Janeiro.

10.1021/jf800467v CCC: $40.75
Published on Web 07/26/2008

in the lipids and proteins associated with the granule starch, there are also differences between granules from the same source, concerning the degree of phosphorylation of the glucosyl residues, depending on the stage of development or ripening of the plant material. All the prior information associated with granule localization, chloroplast or amyloplast, exerts influence on the understanding of the process of starch mobilization. Even the architecture of the native starch granule is still under study, and despite its importance in allowing a better understanding of the mechanism of starch degradation, starch still remains an enigmatic molecule (*5*).

Starch consists mainly of two simple polymers of glucose (amylose and amylopectin), organized to form semicrystalline and insoluble granules. Glucosyl residues in both polymers are linked by α-1,4 and α-1,6 bonds that form chains of variable lengths. Amylopectin is the largest molecule with a branched structure, and amylose is the smallest with very few branched points (α-1,6 bonds). Amylopectin, by far the major component in the known starches, is responsible for the granular semicrystalline structure of starch. In fact, the structure of the starch granule appears to be made up of alternating semicrystalline and crystalline shells. On the basis of their X-ray diffraction patterns, from crystalline shells, granule starch is classified into two major categories named A (mainly cereals starches) and B (found in potato starch and some tropical tubers starches). They mainly differ in the packing of double helices, by the size and the amount of water molecules present in the granule, as well as in their susceptibility to enzyme degradation (*6–10*).

Only few reports on the structure of starches from mango and banana can be found in the literature (*11, 12*). However, the physicochemical, morphological, and rheological properties of these starches are explored as a prospect for food industry utilization (*13, 14*). Not surprisingly, no information is available on the starch granule degradation process during fruit ripening. In this way, the present article presents changes of the physical aspects of the starch granule during mango ripening, through different techniques of microscopy. The results provide clues to gain a better understanding of starch degradation in fruits.

MATERIALS AND METHODS

Materials. Mango fruit (*Mangifera indica* Linn.) was harvested in a plantation located in Joanópolis (São Paulo State, Brazil). The fruits were collected during development at 90, 120, and 180 days after anthesis (daa) immediately frozen in liquid N_2, and stored at −80 °C for future analyses. Mangoes with approximately 207 daa, corresponding to the physiological maturity were stored at temperature (20 °C) and moisture (∼90%) under control, and sampled on a daily basis. The samples were peeled, sliced, and immediately frozen in liquid N_2, and stored at −80 °C for future analyses. At the time of analysis, samples were thoroughly homogenized by powdering in liquid nitrogen. The degree of ripening was monitored through both CO_2 and ethylene levels. Each sample was made by using, at least, 3 mangoes in the same level of respiration and ethylene production. After measuring respiration and ethylene, fruits were cut and frozen as described above.

Ethylene and CO_2 Production. For the evaluation of ethylene production and respiration, the fruit were closed in jars for 1 h and the resulting atmosphere was analyzed by gas chromatography, as previously described by Purgatto et al. (*15*).

Carbohydrates. Soluble sugars from pulp tissue were extracted successively with three volumes of boiling 80% (v/v) aqueous ethanol. The supernatants were combined, and the ethanol was evaporated under vacuum. Sugars were reconstituted in water and analyzed by HPAE-PAD (Dionex, Sunnyvale, CA) using a Carbopac PA-1 column. Starch content was determined as previously described by Cordenunsi and Lajolo (*16*).

Isolation of Starch Granules. Starch was isolated from the samples representative of mango development (180 and 207 daa) and ripening (3, 5, 8, and 10 days after harvest (dah)). Starch granules were isolated according to Ritte et al. (*17*).

Amylose Content. Total amylose content was determined by differential scanning calorimetry according to Mestres et al. (*18*).

Light Microscopy. Dried starch granules were mounted on glass slides using 50% glycerin solution. The starch grains were viewed and photographed using a Zeiss Axioplan 2 (Jena, Germany) microscope with a ColorView XS camera. The length and width of the granules were measured using the software Scion Image. The obtained data were analyzed using the test T Student software Statistica 5.0.

Scanning Electron Microscopy. Dried starch granules were adhered in stubs with double face tape and coated with 20 nm thick gold layer in Balzer's sputtering apparatus. Samples were examined on a Jeol 5310 JSM (Jeol Ltd., Tokyo, Japan) scanning electron microscope for micromorphology analysis (*19*).

Atomic Force Microscopy. A Topometrix Accurex II (Topometrix, Santa Clara, USA) instrument, equipped with a noncontact AFM probe head and a 100 μm Tripod scanner was used to image the samples. The tips (Ultrasharp microprobe) were made of Si and mounted on a cantilever with a spring constant of ca. 40 N/m and resonance frequencies in 100−150 kHz. Scanning was carried out at the free cantilever oscillation frequency and different amplitudes, depending on the stability and contrast, obtained. The amplitude was set higher than 80 nm and the set point was chosen at values around 30% of the free oscillation amplitude in order to guarantee that the microscope was operating in intermittent contact mode. All images were obtained in air. Samples were dispersed in water and a 5 μL drop spread on a piece of silicon wafer. Silicon wafers were treated with oxygen plasma in order to increase its roughness and hydrophilicity prior to starch dispersion. Changes in the sample vertical position are presented as height images. Changes in the phase angle of probe oscillation are presented as phase images.

X-ray Diffraction. X-ray diffractograms of granules were recorded on a PANalytica I diffractometer model X'Pert PRO with detector X'Celerator operating at Cu Kα wavelength of 1.5406 Å. Data were acquired in an angular region of 2.5−70° (2θ) and 0.02°, 5-s steps. The identification of crystalline phases was obtained by comparison to the data from the International Centre for Diffraction Data (2003). Following Hayakawa et al. (*20*), the equation used to determine percentage crystallinity was Crystallinity (%) = $Ac/(Ac + Aa)100$, where *Ac* is the crystalline area on the X-ray diffractogram, and *Aa* is the amorphous area.

RESULTS AND DISCUSSION

Mango Starch Isolation and Characterization. Starch was isolated from 6 representative phases of Keitt development during fruit development (starch accumulation) and during fruit ripening (starch degradation) (**Figure 1**). Starch granules isolated from samples containing the maximum amount of the polysaccharide (zero and 3 days after harvest, ∼7% of starch) were approximately 15 μm in size (**Figure 1**). As ripening proceeded, granule size was reduced to 10 μm by 5 days after harvest (∼6% starch) and approximately 8 μm 8 days after harvest (∼1.5% starch). The medium size of mature-Keitt-starch granules (∼15 μm) was similar to that of the other mango cultivars, such as Criollo and Manila cultivars from Mexico (*21*). However, as can be noticed in **Figure 1**, the shape of Keitt was different from those from the Indian cultivars, which were elliptical in shape. This could be explained by either morphological differences concerning the cultivar or by some degree of degradation in the granule. This hypothesis cannot be excluded since no information about the degree of mango ripeness was reported by the authors.

Keitt mango starch presented A-type X-ray diffraction pattern, with characteristic diffraction peaks at around $2\theta = 15°$, 18°, and 23° as indicated by arrows in **Figure 2**, similar to those of

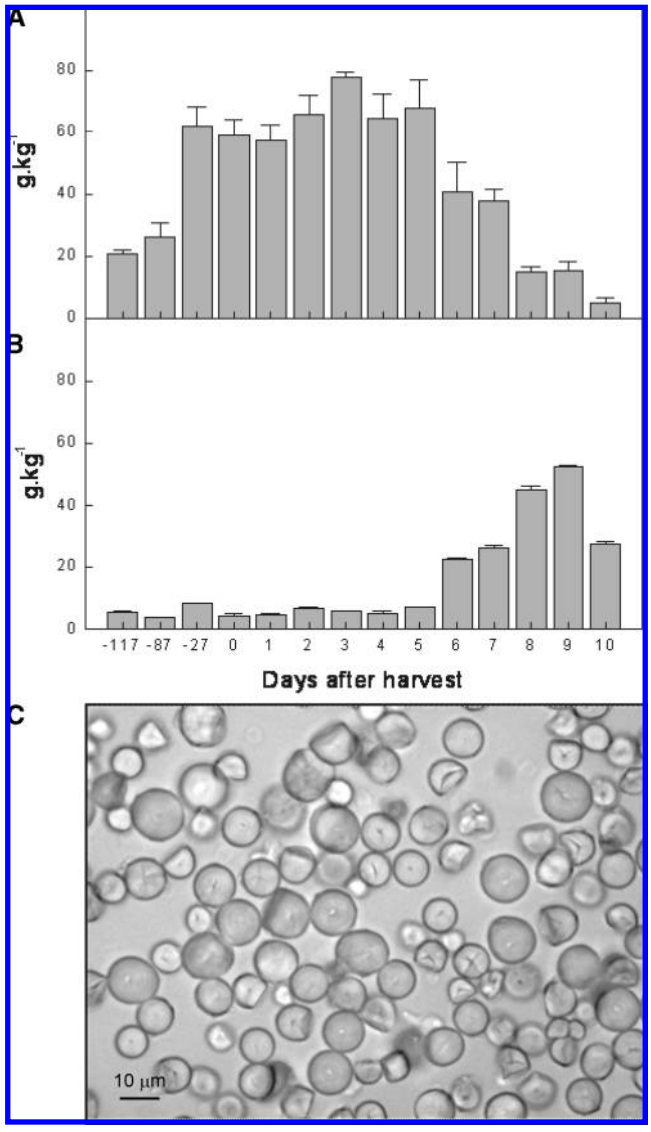

Figure 1. (**A**) Starch and (**B**) sucrose profiles during the development and ripening of Keitt mangoes; (**C**) light microscopy of mature (zero days after harvest) Keitt mango starch granules.

the Mexican cultivars (*21*), and had about 25% of amylose. Usually, type A starches are small in size, presenting a high degree of crystallinity and low or normal (~25%) content of amylose, when compared to that of the B-type. The degree of crystallinity (**Figure 2**) was calculated to be around 21% with a little increase in very degraded starches (day 8-starches).

The SEM-micrograph (**Figure 3A**) from starch isolated from physiologically mature but unripe mangoes (zero days after harvest) showed the predominance of intact spherical granules, covered by what seemed to be one or more incomplete layers, usually round-shaped. Since those pieces of incomplete layers could also be seen in growing granules isolated from undeveloped mangoes (180 days after anthesis), they might be the remains of unfinished new layers covering the starch granule. Some of those incomplete layers were imaged by atomic force microscopy (AFM) and **Figure 3B−D** presents both topographic and phase contrast images of the same region. **Figure 3C** shows the topographic AFM image of the incomplete layer surface presented in **Figure 3A**, showing the presence of 60 nm blocklets. It can be seen that the incomplete layers are around 100 nm in height, which could be an indication of the thickness of a growing ring. Also, the phase contrast image (**Figure 3D**) clearly revealed the presence of fibril-like structures transversally

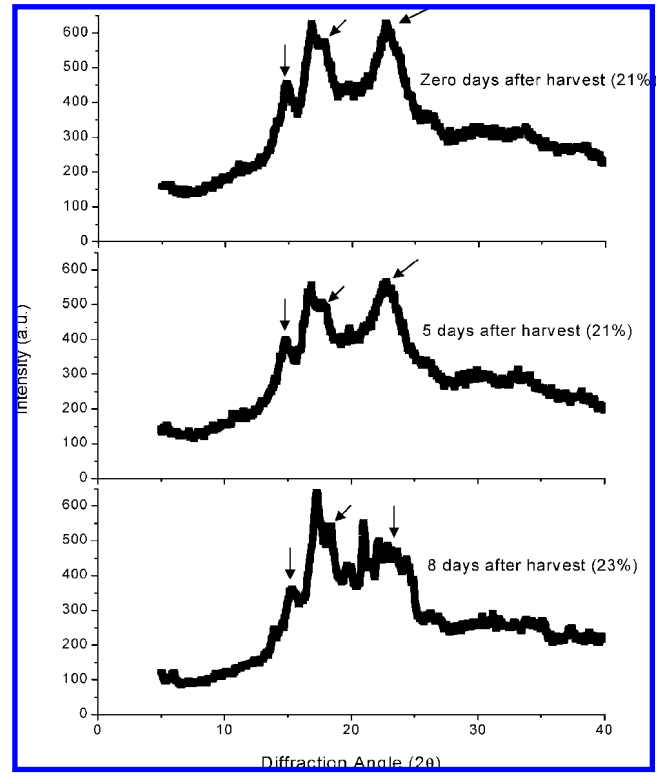

Figure 2. X-ray diffraction patterns of isolated mango Keitt starch. Crystallinity (%) is given in parentheses. The arrows at $2\theta = 15°$, 18°, and 23° indicate diffraction peaks of the A-type allomorph.

connecting the layer to the granule. These fibrils, around 20 nm of diameter, were mainly concentrated in the interface of the layer and the granule surface. In fact, structures with such appearance had never been seen in a starch granule before, and a comprehension of its significance to the structure of the starch granule demands further studies.

It can be observed, in the contrast image (**Figure 3D**), that the fibril-like structure is slightly brighter than the remainder of the surface, having these features marked in the image by arrows, with no direct relationship to the topographic corrugations (**Figure 3C**). Also, dark areas can be seen in the contrast image in between the fibers (**Figure 3D**). The different gray levels observed in phase contrast images can be related to viscoelastic properties of different regions of the sample, similar to the results obtained by Ridout et al. (*9*), who obtained them by imaging the sample with force modulation images. This way, brighter areas in phase contrast images could be related to softer materials, while stiffer areas would appear darker. We can speculate that the presence of two distinct phases on this image can be related to the presence of proteins, more likely to be enzymes involved in the synthesis of the new growing ring.

Apart from this region, the surface of the granule presented a globe-shaped structure, with globules around 60 nm in diameter, as shown in **Figure 3B**. The observed shape and size are similar to the structures described by Baldwin et al. (*22*) on the surface of potato starch granules, which were identified as blocklets. According to the blocklet concept, starch is composed of units of amylopectin arranged in crystalline and amorphous lamellae. The blocklet concept is strongly supported by SEM and AFM studies performed in residual granules of potato and wheat starches, after partial α-amylase hydrolysis (*22*). The less crystalline parts of the granule are more susceptible to a controlled pancreatic α-amylase hydrolysis, resulting in a ghost of the remaining more crystalline regions of the granule, which permits a clear visualization of the blocklets.

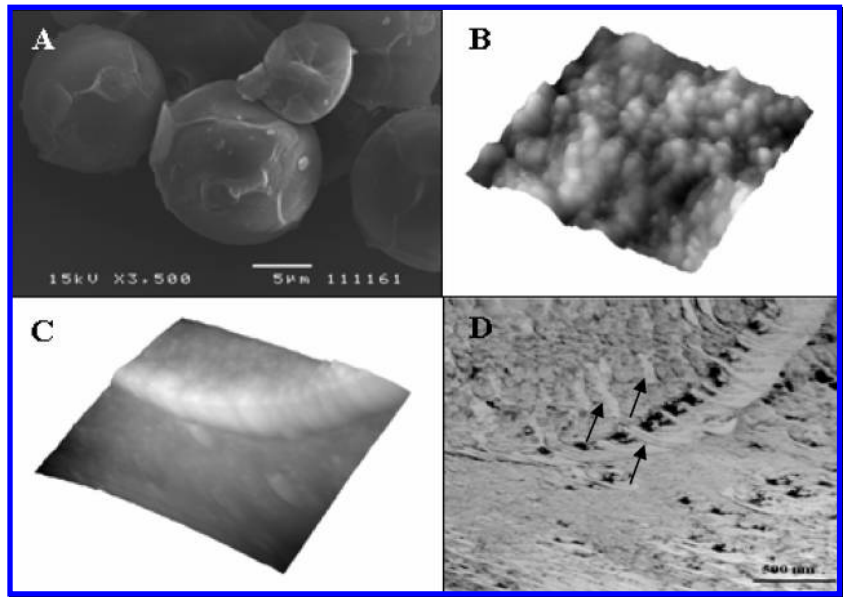

Figure 3. Images of starch granules isolated from mature (zero days after harvest) Keitt mangoes: (**A**) scanning electron microscopy (SEM) image; (**B**) topographic atomic force microscopy (AFM) image of the incomplete layer surface presented in **A**, showing the presence of 60 nm blocklets. Scan size 824 × 824 nm^2; height scale 43 nm. (**C**) 3D representation of atomic force microscopy (AFM) topographic image showing the detail of incomplete layers formed over the granule. Size 2 × 2 μm^2; height scale 360 nm. (**D**) Atomic force microscopy (AFM) phase contrast image of image **B**. Arrows indicate the presence of fibril-like structures.

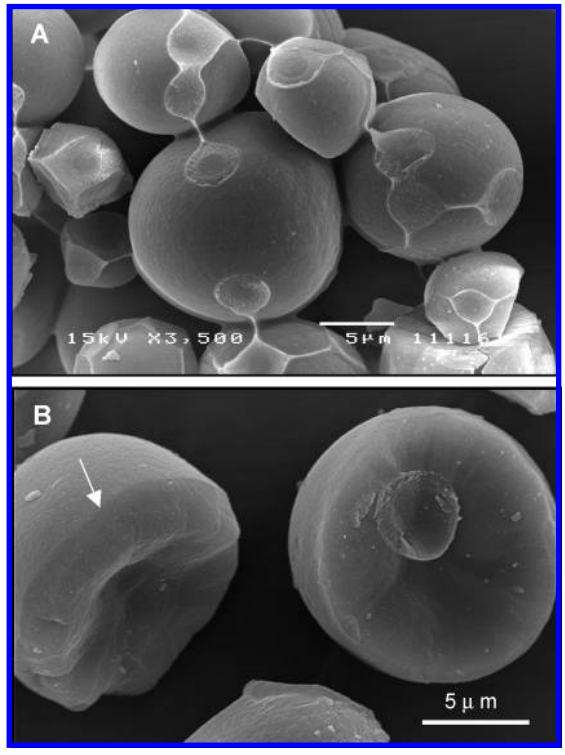

Figure 4. Different scanning electron microscopy (SEM) images of starch granules isolated from Keitt mangoes during ripening (3 days after harvest). The images show granules with different degrees of degradation. The arrow indicates a sharp corner of degradation.

Degradation Pattern As Observed by Microscopy Techniques. The pattern of mango starch degradation seemed not to be dependent on the occurrence of pores on the surface of the granules (**Figure 4**), which is commonly found in maize starch granules. The SEM micrograph showed that the corrosion process did not occur homogeneously along the entire surface. Consequently, the surface seemed to be flatted, and the shape of the original granule was not preserved. A cavity, which may have been formed in the center of each eroded face, drove toward the center granule, indicating that the involved enzymes preferentially degraded it. Data from degree of crystallinity (**Figure 2**) are in agreement with the proposed nonhomogeneous corrosion described here. A small increase in crystallinity could be observed only in late stages of degradation.

The degradation occurring simultaneously in two different points of the same granule resulted in a sharp corner resembling a fracture or a slice as indicated by the arrow (**Figure 4**). These corners were imaged by AFM, and **Figure 5A** and **B** presents topographic and phase contrast images of a step similar to corrosion on the surface. As step height was not uniform along the interface, heights up to 1000 nm could be measured. While the upper part of the step edge seemed to be composed of a homogeneous material, as observed in the phase contrast image (**Figure 5B**), the lower part clearly presented two different phases, which suggests the presence of a surface layer characterized by heterogeneous composition.

The high resolution images of the upper and lower surfaces close to the step presented in **Figure 5C** and **D** indicate that the step-like structure was a result of the degradation process (see the arrow in **Figure 4B** to localize the mentioned degradation seen by SEM). Different structures could be observed either in the lower or the upper part of the corner. The latter presented blocklet-like structures similar to the ones described in **Figure 3B** for the unripe mango (zero days after harvest), and the former part, next to the step, presented a smoother surface composed of elongated features. The observed deformation of the features presented in the upper part of the interface close to the corner could be related only to instrumental limitations. It is likely that the lateral side of the AFM tip touched the edge of the step during scanning.

Several AFM images were obtained on different areas of the degraded granule, and additional information about the corrosion process was obtained by imaging a less corroded surface. **Figure 6** presents AFM images of what seemed to be the initial steps of the corrosion process. Depressions less than 5 nm deep could be seen dispersed on the surface of the granule (**Figure 6A**).

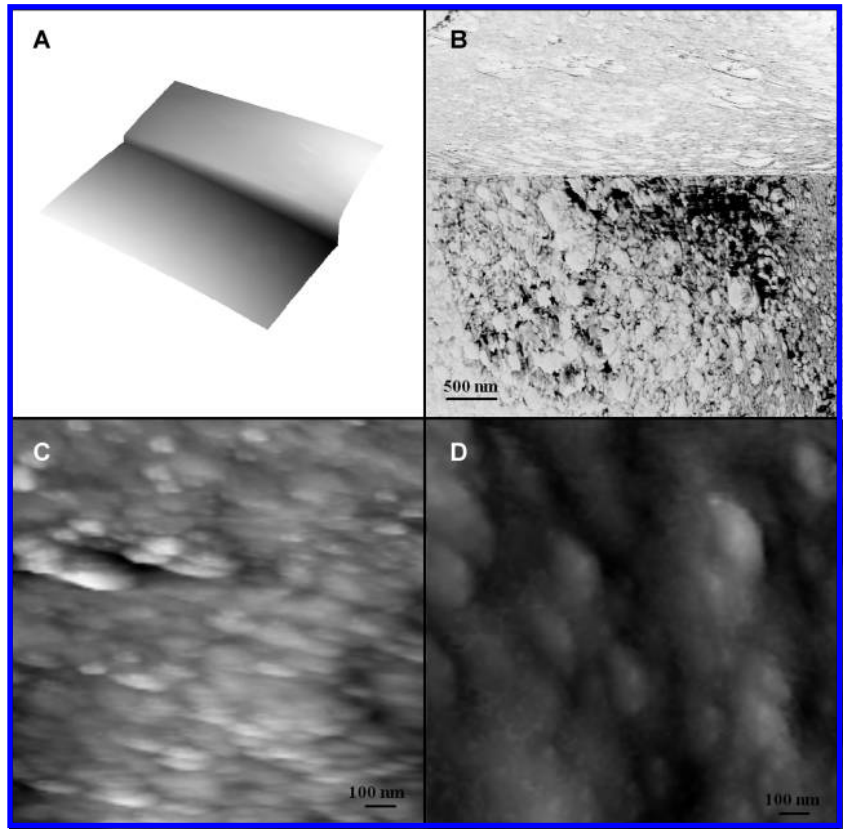

Figure 5. Atomic force microscopy (AFM) images granules starch isolated from Keitt mangoes (3 dah): (**A**) low resolution 3D representation of surface topography. Scan size 4 × 4 μm^2; height scale 4 μm. (**B**) Phase contrast image of **A**. (**C**) Atomic force microscopy (AFM) topographic image showing details of the upper part of the image presented in **A**. (**D**) Details of the lower part of the image presented in **A**. The z scale of images **C** and **D** is 74 nm.

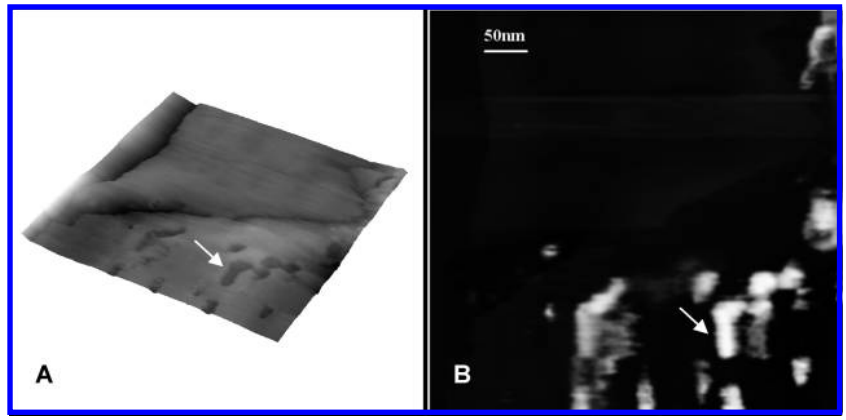

Figure 6. Atomic force microscopy (AFM) high resolution images of the initial stages of *in vivo* degradation of Keitt mango starch after 3 dah: (**A**) 3D representation of the atomic force microscopy (AFM) topographic image. Scan size 830 × 830 nm^2; height scale 23 nm. (**B**) Phase contrast of image presented in **A**. Arrows indicate the pits of corrosion in the surface of the granule.

These depressions are coincident to the regions presenting clear phase contrast (**Figure 6B**), which may indicate the presence of enzymes linked to the starch degradation process. In a parallel work (*18*), α- and β-amylase activities were measured in protein extracts from the same samples of the isolated starch granules. The α-amylase activity and starch content profiles were coincident during mango development and ripening, indicating a high correlation between enzyme activity and the starch degradation process. At the same time, β-amylase activity was barely detectable until day 6, when it started to increase through the end of the starch degradation process. By that day, starch content was 50% lower than the initial one. These activity profiles fit with α-amylase starting the degradation process of the starch granule and producing a substrate for a possible stroma soluble β-amylase. Favoring the first action of α-amylase in the granule, which, rather than other enzymes, starts the degradation process, the pattern of degradation (like pits) presented in **Figure 6** is comparable with patterns presented in the literature (*23*) as a consequence of α-amylase action in the starch granule. Studies of these enzymes immunolocalization in the mango starch granule are under way and will be useful in the subject herein.

The results show, for the first time, details of the natural process of starch granule synthesis and degradation *in loco* by microscopy. During the starch granule synthesis process, fibrillar structures can be seen as well as globular structures named

blocklets. Moreover, the pattern of degradation and information about enzyme activities are favorable to a hydrolytic pathway, first by α-amylase participation and after by β-amylase, with a probable participation of debranching enzymes such as isoamylases.

ACKNOWLEDGMENT

We thank Professor Marcia Attias (Laboratory Ultraestrutura Hertha Meyer from Instituto de Biofísica Carlos Chagas Filho-UFRJ).

LITERATURE CITED

(1) Bernardes-Silva, A. P.; Lajolo, F. M.; Cordenunsi, B. R. *Ciênc. Tecnol. Aliment.* **2003**, *23*, 116–120.
(2) Bernardes-Silva, A. P.; Nascimento, J. R. O.; Lajolo, F. M.; Cordenunsi, B. R. *J. Food Biochem.* **2008**, *32*, 384–395.
(3) Smith, A. M.; Zeeman, S. C.; Smith, S. M. *Annu. Rev. Plant Biol.* **2005**, *56*, 73–97.
(4) Lindeboom, N.; Chang, P. R.; Tyler, R. T. *Starch/Stärke* **2004**, *56*, 89–99.
(5) Zeeman, S. C.; Delatte, T.; Messerli, G.; Umhang, M.; Stettler, M.; Mettler, T.; Streb, S.; Reinhold, H.; Kötting, O. *Funct. Plant Biol.* **2007**, *34*, 465–473.
(6) Gallant, D. J.; Bouchet, B.; Buléon, A.; Pérez, S. *Eur. J. Clin. Nutr* **1992**, *46*, S3-S16.
(7) Oates, C. G. *Trends Food Sci. Technol.* **1997**, *8*, 375–382.
(8) Hedley, C. L.; Bogracheva, T. Y.; Wang, T. L. *Starch/Stärke* **2002**, *54*, 235–242.
(9) Ridout, M. J.; Parker, M. L.; Hedley, C. L.; Bogracheva, T. Y.; Morris, V. J. *Carbohydr. Res.* **2003**, *338*, 2135–2147.
(10) Tester, R. F.; Karkalas, J.; Qi, X. *J. Cereal Sci.* **2004**, *39*, 151–165.
(11) Millan-Testa, C. E.; Mendez-Montealvo, M. G.; Ottenhof, M.-A.; Farhat, I. A.; Bello.Pérez, L. A. *J. Agric. Food Chem.* **2005**, *53*, 495–501.
(12) Zhang, P.; Whistler, R. L.; BeMiller, J. N.; Hamaker, B. R. *Carbohydr. Polym.* **2005**, *59*, 443–458.
(13) Burrell, M. M. *J. Exp. Bot.* **2003**, *54*, 451–456.
(14) Finlay, M.; Dale, B.; Bradshaw, J. E. *Trends Plant Sci.* **2003**, *8*, 310–312.
(15) Purgatto, E.; Lajolo, F. M.; Nascimento, J. R. O.; Cordenunsi, B. R. *J Plant Physiol.* **2002**, *159*, 1105–111.
(16) Cordenunsi, B. R.; Lajolo, F. M. *J. Agric. Food Chem.* **1995**, *43*, 347–351.
(17) Ritte, G.; Lorberth, R.; Steup, M. *Plant J.* **2000**, *2111*, 387–391.
(18) Mestres, C.; Matencio, F.; Pons, B.; Yajid, M.; Fliedel, G. *Starch/Stärke* **1996**, *48*, 2–6.
(19) Louro, R. P.; Santiago, L. J. M.; Dos Santos, A. V.; Machado, R. D. *Trees-Struct. Funct.* **2003**, *17*, 11–22.
(20) Hayakawa, K.; Tanaka, K.; Nakamura, T.; Endo, S.; Hoshino, T. *Cereal Chem.* **1997**, *74*, 576–580.
(21) Bello-Perez, L. A.; Aparicio-Saguilán, A.; Méndez-Montealvo, G.; Solorza-Feria, J.; Flores-Huicochea, E. *Plant Food Hum. Nutr.* **2005**, *60*, 7–12.
(22) Baldwin, P. M.; Adler, J.; Davies, M. C.; Melia, C. D. J. *Cereal Sci.* **1998**, *27*, 255–265.
(23) Buléon, A.; Colonna, P.; Planchot, V.; Ball, S. *Int. J. Biol. Macromol* **1998**, *23*, 85–112.

Received for review February 14, 2008. Revised manuscript received June 17, 2008. Accepted June 20, 2008. This work was supported by FAPESP and CNPq.

JF800467V